Structure and Raman behaviour of $Sm_{2.75}C_{60}$

2000 J. Phys.: Condens. Matter 12 8919

(http://iopscience.iop.org/0953-8984/12/41/318)

J. Phys.: Condens. Matter **12** (2000) 8919–8926. Printed in the UK PII: S0953-8984(00)14470-4

Structure and Raman behaviour of $Sm_{2.75}C_{60}$

Z Sun†‡, X H Chen†‡§, T Takenobu‡ and Y Iwasa‡

† Structure Research Laboratory and Department of Physics, University of Science and Technology of China, Hefei, Anhui 230026, People's Republic of China

‡ Japan Advanced Institute of Science and Technology, Tatsunokuchi, Ishikawa, 923-1292, Japan

Received 6 June 2000, in final form 1 September 2000

Abstract. The structure of $Sm_{2.75}C_{60}$ is determined using the Rietveld method; it is found that $Sm_{2.75}C_{60}$ is isostructural with $Yb_{2.75}C_{60}$. Raman spectra are displayed, and there is an anomalously broad distribution of vibrational structures for the low-frequency H_g modes and around the $A_g(2)$ mode, which can be related to the complexity of the $Sm_{2.75}C_{60}$ structure. The $H_g(2)$ mode is split into five components, allowing a quantitative analysis based on the electron–phonon coupling theory.

1. Introduction

For intercalated fullerides, most donor intercalants are alkali and alkaline-earth metals. The first superconductor found among the rare-earth-doped fullerides, $Yb_{2.75}C_{60}$, was reported by Özdas *et al* [1,2]. $Yb_{2.75}C_{60}$ has a cation-vacancy ordering characteristic, which is responsible for the $Yb_{2.75}C_{60}$ orthorhombic superstructure with space group $Pcab$. Another rare-earth-doped fulleride superconductor, $Sm_{2.75}C_{60}$, was synthesized by Chen and Roth [3] before long. The x-ray diffraction pattern and lattice parameters indicate that $Sm_{2.75}C_{60}$ is isostructural with $Yb_{2.75}C_{60}$. However, a meaningful Rietveld refinement was not carried out in reference [3]. Here, a Rietveld refinement of the $Sm_{2.75}C_{60}$ structure is presented.

Raman scattering is a useful technique for studying the vibrational properties of the C_{60} molecule and its doped derivative compounds. Raman scattering is widely used to evaluate the electron–phonon coupling constant λ for the doped C_{60} superconductors, on the basis of analysis of the linewidths [4–6]. In this paper a quantitative analysis for $Sm_{2.75}C_{60}$ based on the electron–phonon coupling theory is presented.

2. Experiment

A sample of $Sm_{2.75}C_{60}$ was synthesized by reacting stoichiometric amounts of powders of Sm and C_{60}. A quartz tube with mixed powder inside was sealed under a high vacuum of about 2×10^{-6} Torr, and heated at 550–600 °C for three days. X-ray diffraction (XRD) measurement was performed with synchrotron radiation at the beam line BL 1B of the Photon Factory of the National Laboratory for High Energy Physics (KEK-PF, Tsukuba). The synchrotron beam was monochromatized to 1.0006 Å.

The Raman scattering experiment was carried out using the 632.8 nm line of a He–Ne laser in the Brewster-angle back-scattering geometry. The scattering light was detected with a

§ Author to whom any correspondence should be addressed.

0953-8984/00/418919+08$30.00

Dilor XY multichannel spectrometer using a spectral resolution of 3 cm^{-1}. In order to obtain good Raman spectra, the sample was ground and pressed into pellets with a pressure of about 20 kg cm^{-2}, which were sealed in Pyrex tubes under a high vacuum of 10^{-6} Torr.

3. Results and discussion

The x-ray diffraction pattern showed that the sample of $Sm_{2.75}C_{60}$ was single phase, which was also confirmed by the single-peak nature of the pentagonal pinch $A_g(2)$ mode in the Raman spectra.

Figure 1 shows the x-ray diffraction data (crosses) for the sample of $Sm_{2.75}C_{60}$ and our best-fit results (solid line). The XRD pattern was similar to that reported by Özdas *et al* [2]. The refined parameters are summarized in table 1. A least-squares fit was carried out using the GSAS Rietveld refinement with space group *Pcab* (No 61, option 2). Sm cations are located at both tetrahedral (T) and octahedral (O) interstitial sites of the cubic close-packed C_{60} lattice. The initial coordinates of the cations are similar to those of $Yb_{2.75}C_{60}$. All of the O sites are occupied by single Sm cations. One out of every eight T sites in the subcell is vacant, and this vacancy ordering is responsible for the doubling of the unit cell, leading to the formation of superstructure. The Sm cations occupying the O sites and T sites experience off-centre displacement like in the case of $Yb_{2.75}C_{60}$. The Sm cations at the O sites move from the centres of the O sites towards the neighbouring vacancy, while the Sm cations occupying the T sites experience off-centre displacements towards the mid-point between two

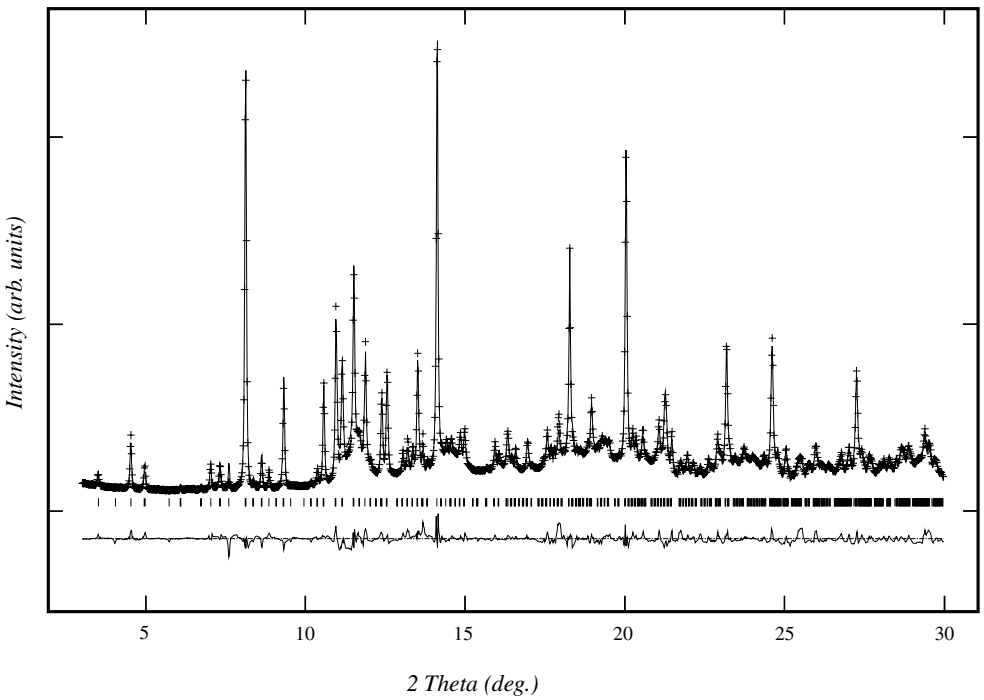

Figure 1. The powder x-ray diffraction pattern of the sample of $Sm_{2.75}C_{60}$ collected with synchrotron radiation. The synchrotron beam was monochromatized to 1.0006 Å. The crosses are experimental points and the solid line is a Rietveld fit to the model of $Sm_{2.75}C_{60}$ in the space group *Pcab* (No 61, option 2). The allowed reflection positions are denoted by ticks.

Table 1. Atomic coordinates, fractional site occupancies N, and thermal factors B for $Sm_{2.75}C_{60}$. The estimated error in the last digit is given in parentheses. Space group $Pcab$ (No 61, option 2), $a = 28.1970(2)$ Å, $b = 28.2350(2)$ Å, $c = 28.1609(2)$ Å.

Atom	Site	x	y	z	B (Å^2)	N
Sm11	8c	0.1236(2)	0.1105(5)	0.3706(3)	0.072(1)	1.00
Sm12	8c	0.3706(3)	0.1236(2)	0.1105(5)	0.072(1)	1.00
Sm13	8c	0.1105(5)	0.3706(3)	0.1236(2)	0.072(1)	1.00
Sm21	8c	0.1236(2)	0.3629(3)	0.3726(4)	0.072(1)	1.00
Sm22	8c	0.3726(4)	0.1236(2)	0.3629(3)	0.072(1)	1.00
Sm23	8c	0.3629(3)	0.3726(4)	0.1236(2)	0.072(1)	1.00
Sm3	8c	0.3759(3)	0.3665(4)	0.3747(3)	0.072(1)	1.00
Sm41	8c	0.2046(1)	0.2046(1)	0.2046(1)	0.046(3)	0.85(1)
Sm42	8c	0.0454(1)	0.0454(1)	0.2046(1)	0.046(3)	0.85(1)
Sm43	8c	0.2046(1)	0.0454(1)	0.0454(1)	0.046(3)	0.85(1)
Sm44	8c	0.0454(1)	0.2046(1)	0.0454(1)	0.046(3)	0.85(1)
Sm51	8c	0.2046(1)	0.2954(1)	0.2954(1)	0.046(3)	0.15(1)
Sm52	8c	0.0454(1)	−0.0454(1)	0.2954(1)	0.046(3)	0.15(1)
Sm53	8c	0.2954(1)	−0.0454(1)	0.0454(1)	0.046(3)	0.30(2)

neighbouring C_{60} molecules, thus decreasing the first-neighbour coordination from four to two C_{60} molecules. The shape of the C_{60} molecules was constrained to icosahedral symmetry. The ratio of the two non-equivalent bond lengths, d_{6-6}/d_{5-6}, was fixed at 1.39 Å/1.45 Å, which is a typical value [7]. The diameter of C_{60} molecules is 7.1 Å. 240 independent carbon atoms define all C_{60} molecules of the superstructure, and their coordinates were reproduced from values reported in reference [7]. The occupancy N of all carbon atoms was fixed as 1. In the process of the refinement, all of the C_{60} molecules were rotated by 37.5° about their local {111} axes in the $Pcab$ space group, just like in the case of $Yb_{2.75}C_{60}$ [2], resulting in a total of 75% of all electron-poor five-membered rings facing cation positions. This structure can be understood within a simple electrostatic energy model [8]. The refinement gave the $R_{wp} = 6.12\%$, $R_p = 4.46\%$ and $\chi^2 = 4.7$. In the difference Fourier map, the highest peak is 1.58 e Å^{-3}, and the deepest hole is -1.59 e Å^{-3}. The lattice parameters were determined to be $a = 28.1970(2)$ Å, $b = 28.2350(2)$ Å, $c = 28.1609(2)$ Å. The calculated density was 2.69 g cm^{-3}; the volume was 22 420 Å^3.

The lattice parameters for the sample of $Sm_{2.75}C_{60}$ are significantly larger than those of $Yb_{2.75}C_{60}$ ($a = 27.874$ Å, $b = 27.980$ Å, $c = 27.873$ Å). For $Yb_{2.75}C_{60}$, the oxidation state of Yb is +2, which is supported by near-edge and extended x-ray absorption fine-structure measurements [2]. The ionic radius of Yb^{2+} is larger than that of Sm^{3+}, but smaller than that of Sm^{2+}. Therefore the large lattice parameters for $Sm_{2.75}C_{60}$ indicate that the Sm in $Sm_{2.75}C_{60}$ is also divalent. In Raman spectra of $Sm_{2.75}C_{60}$, the $A_g(2)$ mode gives further evidence that Sm is divalent, which will be mentioned below.

Figure 2 displays the room temperature Raman spectra of $Sm_{2.75}C_{60}$. The positions (ω) and halfwidths (γ) of the Raman modes observed are listed in table 2. For comparison, the lines for pure C_{60} are included in table 2. An anomalously broad distribution of vibrational structures for the low-frequency H_g modes and around the $A_g(2)$ mode can be observed, which can be related to the complexity of the $Sm_{2.75}C_{60}$ structure. Citrin *et al* reported a similar distribution of vibrational structures around the $A_g(2)$ mode for $Yb_{2.75}C_{60}$ [9]. However, in the Raman

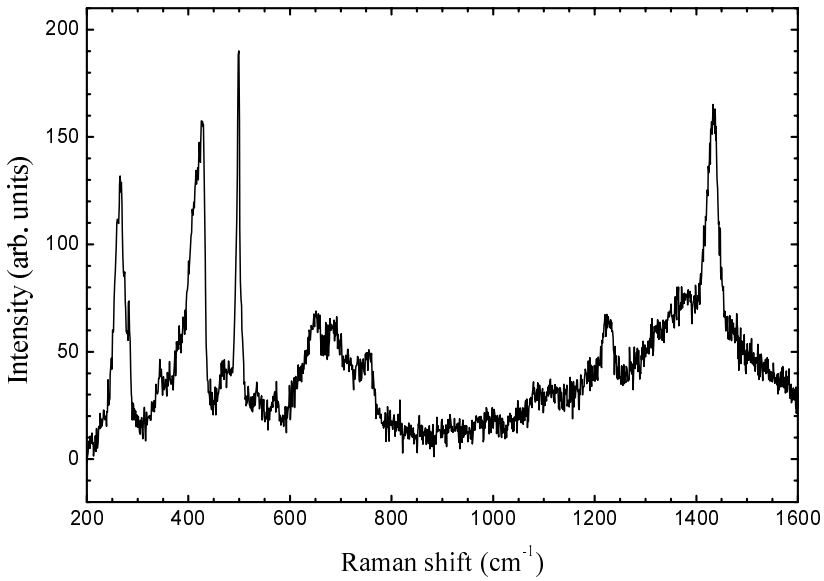

Figure 2. Room temperature Raman spectra of $Sm_{2.75}C_{60}$.

Table 2. Positions and linewidths for the Raman modes in $Sm_{2.75}C_{60}$ as related to C_{60}.

	C_{60}	$Sm_{2.75}C_{60}$	
I_h mode	ω (cm^{-1})	ω (cm^{-1})	γ (cm^{-1})
$A_g(1)$	493	498.3	6.9
$A_g(2)$	1469	1432.8	22.6
$H_g(1)$	270	264.7	23.3
		283.0	3.1
$H_g(2)$	431	342.9	45.2
		386.7	34.7
		407.6	19.7
		418.9	13.9
		428.2	7.9
$H_g(3)$	709	647.9	25.0
		683.4	31.0
$H_g(4)$	773	756.7	23.0
$H_g(5)$	1099	1085.5	22.3
		1112.4	12.8
$H_g(6)$	1248	1226.2	20.9
$H_g(7)$	1426	1387.8	46.0
$H_g(8)$	1573		

spectra of $Sm_{2.75}C_{60}$, there are no discrete modes around the $A_g(2)$ mode, which were observed for $Yb_{2.75}C_{60}$ and considered as evidence of the existence of distorted C_{60} molecules [9]. For doped fullerides, the doping process leads to a characteristic downshift of the $A_g(2)$ mode as

regards the number of electrons transferred to the C_{60} molecule. A downshift of 6–7 cm^{-1} per elementary charge on C_{60}, independent of the doping ions, is observed [10–14]. For $Sm_{2.75}C_{60}$, the pinch $A_g(2)$ mode occurs at 1432.8 cm^{-1}, which indicates that Sm is divalent and the charge transfer is complete, according to a 6.3 cm^{-1} red-shift per electron relative to neutral C_{60}.

The low-frequency $H_g(1)$ and $H_g(2)$ modes are asymmetric. A bunch of lines appears around 700 cm^{-1} that are probably to be assigned to the $H_g(3)$ and $H_g(4)$ modes. The $H_g(8)$ mode cannot be derived from the anomalously broad distribution of vibrational structures around the $A_g(2)$ mode. Figure 3 shows the result of a line-shape analysis of the Raman spectra of the $H_g(2)$ mode. The $H_g(2)$ mode has to be fitted with five components. This suggests that the degeneracy of the $H_g(2)$ mode is lifted. This splitting may be attributed to the symmetry lowering due to the orthorhombic superstructure of this material. A similar behaviour has been observed for single-crystal K_3C_{60} at 80 K [6] and for Ba_4C_{60} and Ba_6C_{60} at room temperature [15].

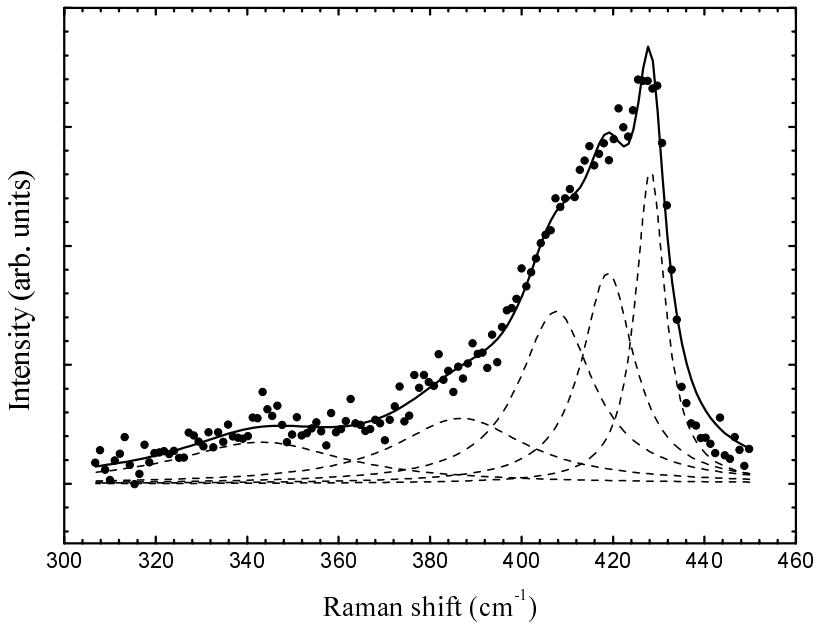

Figure 3. Raman spectra of the $H_g(2)$ mode for $Sm_{2.75}C_{60}$. The dotted lines are computer fits for the individual components, which add up to the solid line through the experimental points.

The $H_g(2)$ mode of $Sm_{2.75}C_{60}$ shows a strong peak at the high-frequency edge associated with a long-tailed structure towards lower frequencies. A clear relation between the line shift and line broadening can be observed. Winter and Kuzmany have pointed out that the electron–phonon interaction plays an important role in the broadening and the shift of the lines, and they deduced electron–phonon coupling constants for K_3C_{60} [6]. The phonon linewidth γ_i due to the electron–phonon interaction in a metal can be related to a dimensionless electron–phonon coupling constant λ_i given by

$$\gamma_i = \frac{1}{g_i}\frac{\pi}{2}N(0)\lambda_i\omega_{bi}^2 \tag{1}$$

where for each of the modes γ_i is the full width at half-maximum (FWHM) of the line, $N(0)$ is the density of states at the Fermi level per spin and molecule, and g_i and ω_{bi} are the mode

degeneracy and the frequency prior to any coupling to the electrons, respectively. Allen's formula given above will be used to derive the coupling constants for the eight H_g modes. The frequencies of pure C_{60} were used as the bare-phonon frequencies. In the framework of Allen's theory, there should be a linear relation of the form

$$\gamma = -\frac{\pi}{2} N(0)\omega_b \, \Delta\omega \tag{2}$$

between γ the linewidth and $\Delta\omega$ the difference between the bare-phonon frequency and the observed frequency. The relation between linewidth and frequency shift, according to the experimental values of the $H_g(2)$ mode given in table 2, is plotted in figure 4. In agreement with equation (2), the relation between γ and $\Delta\omega$ is linear. $N(0)$ can be deduced from the slope of the line. The density of states obtained from the $H_g(2)$ mode is 5.8 eV^{-1}. This value is used for $N(0)$ in order to evaluate the coupling constants. The averaged linewidths and the overall coupling constants for each mode except the $H_g(8)$ mode and for all H_g modes are listed in table 3, together with the frequencies for pure C_{60}. Generally, the contribution from the $H_g(8)$ mode to the overall coupling constant is very small, so neglecting the $H_g(8)$ mode could not affect our result. The averaged linewidths are directly evaluated from the linewidths listed in table 2. The values for λ_i are obtained using equation (1).

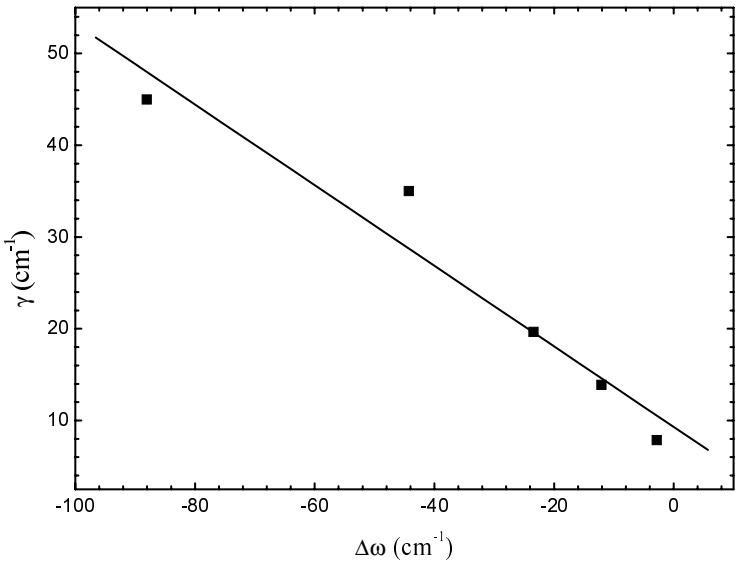

Figure 4. A plot of the linewidth γ versus the observed frequency shift $\Delta\omega$ for the individual components of the $H_g(2)$ mode for the sample of $Sm_{2.75}C_{60}$.

In table 3, the individual contributions to the coupling constant from each H_g mode are listed. The two lowest-frequency H_g modes dominate the contribution to λ, yielding about 70% of the total value. Within the BCS framework, the superconducting transition temperature T_c can be evaluated on the basis of the experimental values for λ by using the McMillan equation:

$$T_c = \frac{\hbar\omega_{ln}}{1.2k_B} \exp\left[\frac{-1.04(1+\lambda)}{\lambda - \mu^* - 0.62\lambda\mu^*}\right] \tag{3}$$

where ω_{ln} is the logarithmically averaged phonon frequency, k_B is the Boltzmann constant, and μ^* is the Coulomb repulsion between conduction electrons. According to the observed frequencies and the evaluated coupling constants, ω_{ln} was determined as 450 cm^{-1}. With this

Table 3. Positions, averaged linewidths, and electron–phonon coupling constants normalized to the density of states at the Fermi energy for eight fivefold-degenerate H_g modes for the $Sm_{2.75}C_{60}$ sample.

Modes	ω (cm^{-1})	$\overline{\gamma}$ (cm^{-1})	$\lambda/N(E_F)$
$H_g(1)$	270	13.2	0.137
$H_g(2)$	431	24.3	0.099
$H_g(3)$	709	28.0	0.042
$H_g(4)$	773	23.0	0.029
$H_g(5)$	1099	17.5	0.011
$H_g(6)$	1248	20.9	0.010
$H_g(7)$	1426	46.0	0.017
$H_g(8)$	1573		
$\sum$			0.345

value and λ, a superconducting transition temperature of 8 K can be evaluated, assuming the μ^*-value to be 0.31, which is similar to the value 0.3 for Ba_4C_{60} [15] but much larger than the value 0.18 for K_3C_{60} [6], in the same way as for the evaluation of T_c.

4. Conclusions

The structure of $Sm_{2.75}C_{60}$ is identical to that of $Yb_{2.75}C_{60}$. These two rare-earth-doped fullerides have the same cation-vacancy ordering characteristic. There is an anomalously broad distribution of vibrational structures for the low-frequency H_g modes and around the $A_g(2)$ mode, which can be related to the complexity of the $Sm_{2.75}C_{60}$ structure. The $H_g(2)$ mode is split into five components. A characteristic relation between the line shift and linewidth is observed and used to evaluate $N(0)$. The electron–phonon coupling constants are evaluated on the basis of the Raman results in the framework of Allen's theory.

Acknowledgments

We would like to acknowledge Y Murakami for help with the synchrotron x-ray diffraction measurements. This work was supported by a grant from the Natural Science Foundation of China.

References

[1] Özdas E, Kortan A R, Kopylov N, Glarum S M, Haddon R C, Fleming R M and Ramirez A P 1993 *Proc. Mtg of the Materials Research Society (Fall 1993)* (Pittsburgh, PA: Materials Research Society)
[2] Özdas E, Kortan A R, Kopylov N, Ramirez A P, Siegrist T, Rabe K M, Bair H E, Schuppler S and Citrin P H 1995 *Nature* **375** 126
[3] Chen X H and Roth G 1995 *Phys. Rev.* B **52** 15 534
[4] Mitch M G, Chase S J and Lannin J S 1992 *Phys. Rev. Lett.* **68** 883
[5] Zhou P, Wang K A, Eklund P C, Dresselhaus G and Dresselhaus M S 1993 *Phys. Rev.* B **48** 8421
[6] Winter J and Kuzmany H 1996 *Phys. Rev.* B **53** 655
[7] Zhou O and Cox D E 1992 *J. Phys. Chem. Solids* **53** 1373
[8] Rabe K M and Citrin P H 1998 *Phys. Rev.* B **58** 551
[9] Citrin P H, Özdas E, Schuppler S, Kortan A R and Lyons K B 1997 *Phys. Rev.* B **56** 5213
[10] Haddon R C, Hebbard A F, Rosseinsky M J, Murphy D W, Duclos A J, Lyons K B, Miller B, Rosamilia J M, Fleming R H, Kortan A R, Glarum S H, Makhga A V, Muller A J, Eick R H, Zahurak S M, Tycko R, Dabbah G and Thiel F A 1991 *Nature* **350** 320

[11] Duclos S J, Haddon R C, Glarum S H, Hebbard A F and Lyons K B 1991 *Science* **254** 1625
[12] Pichler T, Matus M, Kürti J and Kuzmany H 1992 *Phys. Rev.* B **45** 13 841
[13] Wang K A, Wang Y, Zhou P, Holden J M, Ren S L, Hager G T, Ni H F, Eklund P C, Dresselhaus G and Dresselhaus M S 1992 *Phys. Rev.* B **45** 1955
[14] Kuzmany H, Matus M, Burger B and Winter J 1994 *Adv. Mater.* **6** 731
[15] Chen X H, Taga S and Iwasa Y 1999 *Phys. Rev.* B **60** 4351